Electronic Supplementary Material (ESI) for Lab on a Chip.

Continuous-Flow Macromolecular Sieving in Slanted Nanofilter Array: Stochastic Model and Coupling Effect of Electrostatic and Steric Hindrance

*Sung Hee Ko[a] *, Pyeong Jun Park[b] * & Jongyoon Han[c,d]*

1. Slanted nanofilter array chip

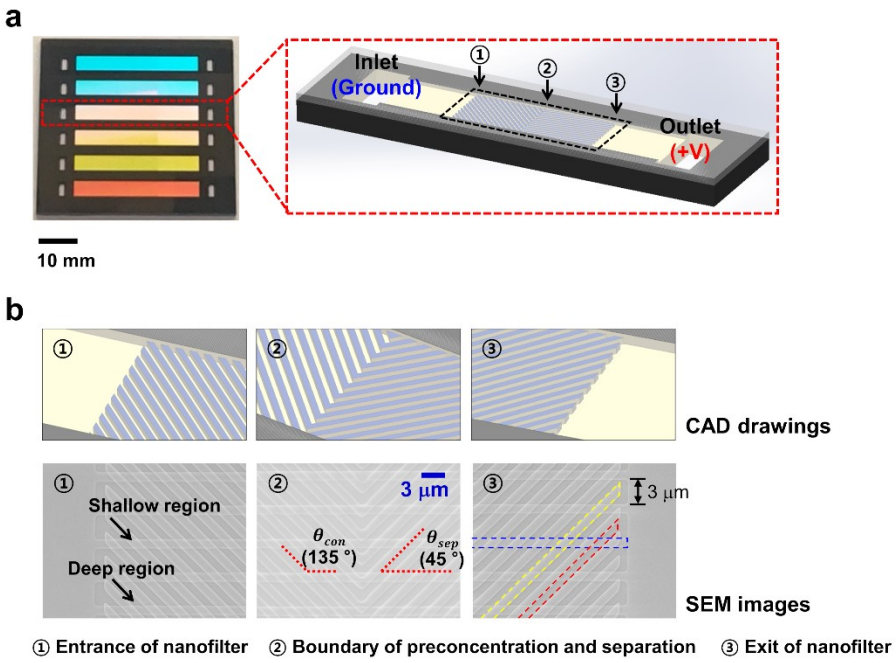

Supplementary Fig. S1. Schematics of slanted nanofilter array. (a) A slanted nanofilter array device consisting of six multiple channels in a single silicon-glass chip. Drawing of the single channel with one inlet and one outlet. (b) CAD drawings and SEM images presenting details of the slanted nanofilter structure. Entrance of nanofilter array ①, the boundary of concentration region and separation region ②, and exit of nanofilter array (separation region) ③. Arrows in ① SEM image indicate paths of deep and shallow regions. θ_{con}: nanofilter angle in the concentration region and θ_{sep}: nanofilter angle in the separation region, which is the same as the nanofilter angle θ_N in the main text. Nanofilter structures in both concentration and separation regions are symmetric. Scale bar is 3 μm. Dashed lines in ③ SEM image are outlines of deep nanochannel (red line, 1 μm wide), supporting wall to prevent nanochannel collapse (blue line, 1 μm wide), and shallow nanochannel (yellow line, 1 μm wide). The width between supporting walls (blue dashed line) is 3 μm.

The SNA fabricated by glass-silicon bonding is divided into two regions with dissimilar nanofilter angles, called sample concentration and separation regions (Fig. S1). Driven by electrophoretic forces, negatively charged macromolecules enter the nanofluidic device and migrate through the nanofilter arrays. To apply electrophoretic force effectively, we used a high ionic strength buffer to suppress electroosmotic flow (dominant driver at low ionic strength) and ion concentration polarization (phenomenon occurring at the interface between bulk and charged nanosized pores) [1], which would interfere with the electrophoretic motion of macromolecules. In the concentration region, macromolecules of different sizes are focused on the bottom side of the wall by the slanted interface between the deep and shallow regions, causing all the macromolecules to be located at the same position and concentrated before entering the separation region. The focused macromolecules are then size-separated in the separation region (Fig. 1a in main text) [2].

2. Stochastic model for molecule dynamics in slanted nanofilter array

To study the dynamics of a molecule in a nanofilter array, we considered a master equation for the probability of the molecule position. The dynamics of a molecule is described by the time evolution of $P_D(n, y, t)$ and $P_S(n, y, t)$ which are defined by the probability that a molecule exists at position y in the n-th deep and shallow regions, respectively, at time t. The time evolutions of $P_D(n, y, t)$ and $P_S(n, y, t)$ are described by the following master equation:

$$\left(\frac{\partial}{\partial t} - L_D\right)P_D(n,y,t) = w_S^+ P_S(n-1,y,t) + w_S^- P_S(n,y,t) - (w_D^+ + w_D^-)P_D(n,y,t)$$

* MERGEFORMAT (1)

$$\left(\frac{\partial}{\partial t} - L_S\right)P_S(n,y,t) = w_D^+ P_D(n-1,y,t) + w_D^- P_D(n,y,t) - (w_S^+ + w_S^-)P_S(n,y,t)$$

₩* MERGEFORMAT (2)

where L_D and L_S are the time evolution operators associated with the dynamics in the y direction in the deep and shallow regions, respectively, given by

$$L_D = D\frac{\partial^2}{\partial y^2} - v_y^D\frac{\partial}{\partial y}$$

* MERGEFORMAT (3)

*
ME
RG
EF
OR
MA
T

$$L_S = D\frac{\partial^2}{\partial y^2} - v_y^S\frac{\partial}{\partial y} \quad (4)$$

where D is the diffusion coefficient of a molecule. $v_y^D = \frac{QE_y^D}{f}$ and $v_y^S = \frac{QE_y^S}{f}$ are the drift velocities of the molecule in the deep and shallow regions, respectively, in the y direction, where Q is the magnitude of the effective charge of the molecule ($Q > 0$). E_y^D and E_y^S are the electric field strengths in the y direction, and f is the friction coefficient of the molecule. $w_D^{\pm}$ and $w_S^{\pm}$ are the transition rates from the deep and shallow regions to the neighboring shallow and deep regions, respectively. Using the Fourier-Laplace transform defined by

*
MERGEFORMAT

$$P_D(n,k,s) = \int_0^{\infty} dt e^{-st} \int_{-\infty}^{\infty} dy e^{-iky} P_D(n,y,t)$$

(5)

*
MERGEFORMAT

$$P_S(n,k,s) = \int_0^{\infty} dt e^{-st} \int_{-\infty}^{\infty} dy e^{-iky} P_S(n,y,t)$$

(6)

time evolution equations (1) and (2) are decoupled as

$$\left[\hat{\mathcal{L}}_D - \frac{w_S^+ w_D^- + w_D^+ w_S^-}{\hat{\mathcal{L}}_S}\right] P_D(n,k,s) = \delta_{n,n_0} e^{-iky_0} + \frac{w_S^+ w_D^+}{\hat{\mathcal{L}}_S} P_D(n-1,k,s) + \frac{w_S^- w_D^-}{\hat{\mathcal{L}}_S} P_D(n+1,k,s) \quad (7)$$

$$\left[\hat{\mathcal{L}}_S - \frac{w_S^+ w_D^- + w_D^+ w_S^-}{\hat{\mathcal{L}}_D}\right] P_S(n,k,s) = \frac{w_S^+ w_D^+}{\hat{\mathcal{L}}_D} P_S(n-1,k,s) + \frac{w_S^- w_D^-}{\hat{\mathcal{L}}_D} P_S(n+1,k,s) \quad (8)$$

where $\hat{\mathcal{L}}_D = s + w_D^- + w_D^+ + k^2 D + ikv_y^D$ and $\hat{\mathcal{L}}_S = s + w_S^- + w_S^+ + k^2 D + ikv_y^S$, and the following initial conditions were used:

$$P_D(n, y, t = 0) = \delta_{n,n_0}\delta(y - y_0) \quad (9)$$

$$P_S(n, y, t = 0) = 0 \quad (10)$$

Assuming $\bar{w_D} = \bar{w_S} = 0$, we can obtain the following solution of the coupled master equations:

$$P_D(n,k,s) = \frac{\left(w_S^+ w_D^+\right)^n}{\left(s + w_D^+ + k^2 D + ikv_y^D\right)^{n+1}\left(s + w_S^+ + k^2 D + ikv_y^S\right)^n} \quad (11)$$

$$P_S(n,k,s) = \frac{\left(w_S^+\right)^n \left(w_D^+\right)^{n+1}}{\left(s + w_D^+ + k^2 D + ikv_y^D\right)^{n+1}\left(s + w_S^+ + k^2 D + ikv_y^S\right)^{n+1}} \quad (12)$$

By performing the inverse Fourier-Laplace transform, $P_D(n, y, t)$ and $P_S(n, y, t)$ can be obtained as

$$P_D(n,y,t) = \frac{\left(w_S^+ w_D^+\right)^n}{n!(n-1)!}\int_0^t dt' \frac{(t')^{n-1}(t-t')^n e^{-w_S^+ t' - w_D^+ (t-t')}}{\sqrt{4\pi D t}} e^{-\frac{\left(y - v_y^S t' - v_y^D (t-t')\right)^2}{4Dt}} \quad (13)$$

$$P_S(n,y,t) = \frac{\left(w_S^+\right)^n \left(w_D^+\right)^{n+1}}{(n!)^2}\int_0^t dt' \frac{(t')^n (t-t')^n e^{-w_S^+ t' - w_D^+ (t-t')}}{\sqrt{4\pi D t}} e^{-\frac{\left(y - v_y^S t' - v_y^D (t-t')\right)^2}{4Dt}} \quad (14)$$

After the transient periods, the asymptotic mean and variance of the molecule position are given by

$$\langle x(t)\rangle = \frac{w_S^+ w_D^+}{w_S^+ + w_D^+}(l_S + l_D)t \quad (15)$$

$$\langle x(t)^2\rangle - \langle x(t)\rangle^2 = \frac{w_S^+ w_D^+ \left(\left(w_S^+\right)^2 + \left(w_D^+\right)^2\right)}{\left(w_S^+ + w_D^+\right)^3}(l_S + l_D)^2 t \quad (16)$$

$$\langle y(t)\rangle = \frac{v_y^S w_D^+ + v_y^D w_S^+}{w_S^+ + w_D^+}t \quad (17)$$

$$\langle y(t)^2 \rangle - \langle y(t) \rangle^2 = 2\left[D + \frac{w_S^+ w_D^+ \left(v_y^D - v_y^S\right)^2}{\left(w_S^+ + w_D^+\right)^3}\right]t$$ * MERGEFORMAT (18)

where l_D and l_S are the pitches of each deep and shallow region (Fig. 1d in the main text), and $\langle x \rangle$ and $\langle y \rangle$ are the ensemble averages. The deflection angle θ_M from the *x*-axis defined in Fig. 1c in the main text is then given by:

$$\tan \theta_M = \frac{\langle y \rangle}{\langle x \rangle} = \frac{v_y^S w_D^+ + v_y^D w_S^+}{w_S^+ w_D^+ \left(l_S + l_D\right)}$$ * MERGEFORMAT (19)

To determine the deflection angle in terms of experimental parameters, we identified the transition rates as follows: the inversion of w_D^+ and w_S^+ is given by

$$\frac{1}{w_D^+} = \frac{l_D}{v_x^D} + \frac{1}{k_D^+} \quad (20)$$

$$\frac{1}{w_S^+} = \frac{l_S}{v_x^S} + \frac{1}{k_S^+} \quad (21)$$

where $v_x^D = \frac{QE_x^D}{f}$ and $v_x^S = \frac{QE_x^S}{f}$ are the drift velocities in the deep and shallow regions in the x direction, respectively, and E_x^D and E_x^S are the electric field strengths in the x direction. k_D^+ and k_S^+ are the escape rates from deep or shallow regions to their neighboring regions in the $+x$ direction. Because there is no barrier to molecules moving from shallow to deep, we assumed $\frac{1}{k_S^+} \to 0$. Therefore, the deflection angle from the x-axis can be expressed in terms of k (replacing k_D^+ with k) as follows:

* MERGEFORMAT

$$\tan\theta_M = \tan\theta_E + \frac{QE_y^D}{(l_D + l_S)fk} \quad (22)$$

where θ_E is the direction of the external electric field. The electric field strength is defined as follows:

* MERGEFORMAT

$$E_x^D = E_0^D \cos\theta_E = \left(\frac{2d_S}{d_D + d_S}\right) E_0 \cos\theta_E \quad (23)$$

$$E_y^D = E_0^D \sin\theta_E = \left(\frac{2d_S}{d_D + d_S}\right) E_0 \sin\theta_E \quad \text{(24)}$$

$$E_x^S = E_0^S \cos\theta_E = \left(\frac{2d_D}{d_D + d_S}\right) E_0 \cos\theta_E \quad \text{(25)}$$

$$E_y^S = E_0^S \sin\theta_E = \left(\frac{2d_D}{d_D + d_S}\right) E_0 \sin\theta_E \quad \text{(26)}$$

where E_0 is the average strength of the external electric field. In Eq. (22), the first term is due to free draining, and the second term is due to the molecule movement in the y direction during the

trapping time in the deep region; the larger the molecule size, the larger the deflection angle and trapping time.

3. Steric partition coefficient in the nanofilter array

By statistical thermodynamics, the steric partition coefficient of a DNA can be written as

$$K_{Steric} = \left(\frac{d_S}{d_D}\right)\frac{K_S}{K_D} \tag{27}$$

where K_S and K_D that are each partition function for shallow region and deep region for a rod-like DNA with length L are given by

$$K_S = \begin{cases} 1 - \dfrac{L}{2d_S}, & L \le d_S \\ \dfrac{d_S}{2L}, & L > d_S \end{cases} \tag{28}$$

$$K_D = \begin{cases} 1 - \dfrac{L}{2d_D}, & L \le d_D \\ \dfrac{d_D}{2L}, & L > d_D \end{cases} \tag{29}$$

where width of nanochannel (w) is much larger than depth of nanochannel (d) ($w \gg d$, slit-pore). When the contour length of the DNA (L_c) is longer than the persistence length (L_p), L can be replaced with end-to-end distance calculated from worm-like chain model (Kratky-Porod model)

$$L = \left[2L_cL_p\left\{1 - \frac{L_p}{L_c}\left(1 - e^{-L_c/L_p}\right)\right\}\right]^{1/2}. \tag{30}$$

The asymptotic form of K_{steric} is given by d_S/d_D for the end-to-end distance of DNA much smaller than d_S and d_D (L is almost zero), and by $(d_S/d_D)^2$ for the distance of DNA larger than d_S and

d_D. In this study, we note that persistence length and contour length per base pair of DNA are 50 nm and 0.34 nm/bp, respectively.

4. Effect of buffer ionic strength on molecule deflection in slanted nanofilter array

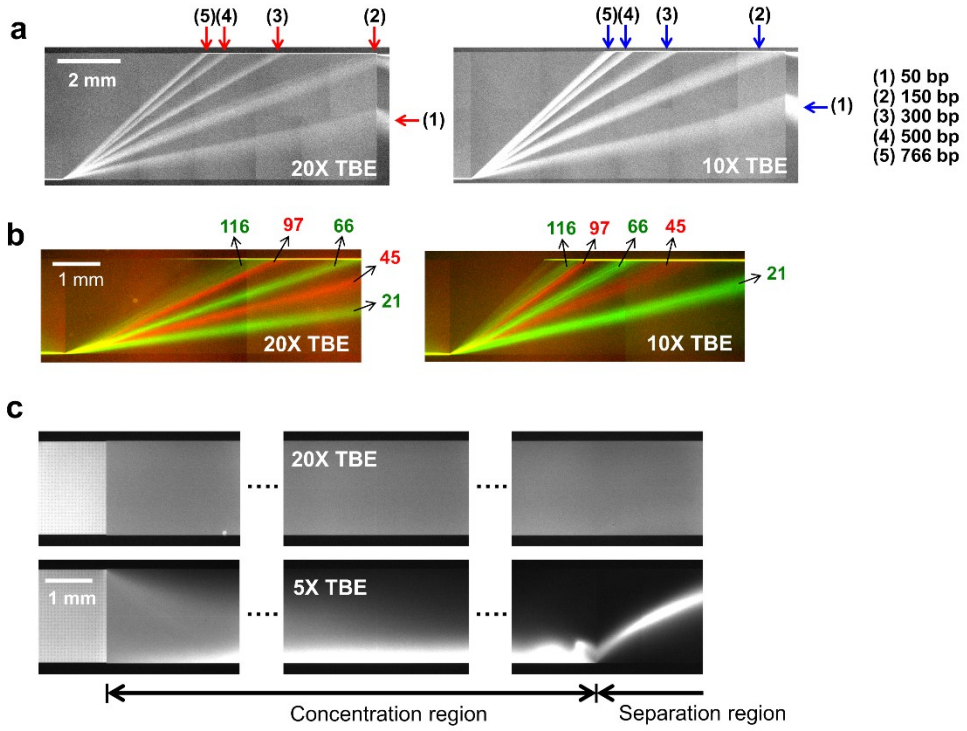

Supplementary Fig. S2. Effect of buffer ionic strength on molecular transport in the SNA. (a) DNA stream deflection in 20 X and 10 X of TBE. DNA size: 50 bp (1), 150 np (2), 300 bp (3), 500 bp (4) and 766 bp (5). d_S= 30 nm, d_D= 100 nm, θ_N= 45° and E_0= 33.3 V/cm. Scale bar is 2 mm. (b) SDS-denatured protein stream deflection in 20 X and 10 X of TBE. Protein size: 21 kDa, 45 kDa, 66 kDa, 97 kDa, and 116 kDa. Proteins were labeled by two fluorescence dyes with different excitation/emission wavelengths (green stream: Alexa Fluor 488, red stream: Alexa Fluor 555). d_S= 25 nm, d_D= 100 nm, θ_N= 45° and E_0= 33.3 V/cm. Scale bar is 1 mm. (c) Fluorescence dye molecule (fluorescein, ~ 332.3 Da) stream deflection angle in 20 X and 5 X of TBE. d_S= 60 nm, d_D= 120 nm, θ_N= 45° and E_0= 33.3 V/cm. Scale bar is 1 mm.

To investigate the electrostatic interaction between the charged molecule and nanofilter wall under high ionic strength conditions, we observed changes in the molecular behavior depending on the buffer ionic strength (Supplementary Fig. 2). In conventional studies, electrostatic interactions between the solute and nanofilter have been ignored when a high ionic strength buffer is used because most surface charges are screened under high ionic strength conditions. However, experiments have shown that the deflection of molecules in the slanted nanofilter array is affected by ionic strength, despite the buffer ionic strengths being high. Deflection angles of DNA and SDS-denatured proteins in 10X TBE are larger than 20X TBE, owing to high electrostatic repulsion [3]. Some publications have reported that DNA size increases with decreasing ionic strength [4-6]; thus, change in deflection is possibly caused by the size difference. However, a noticeable change in size by ionic strength, which can affect molecule deflection, was observed in large DNA over a few kilobase pairs, but not in the small DNA used in this study. To provide further assurance that the impact of the electrostatic interaction is critical, we used a fluorescence dye (fluorescein) and a large nanofilter array to exclude the effect of the molecular physical size. As a result of the change in the deflection of the dye molecule depending on the ionic strength, we concluded that electrostatic repulsion between charged molecules and the nanofilter wall play a critical role, even under high ionic strength conditions.

5. DNA stream deflection angles depending on DNA size for various conditions

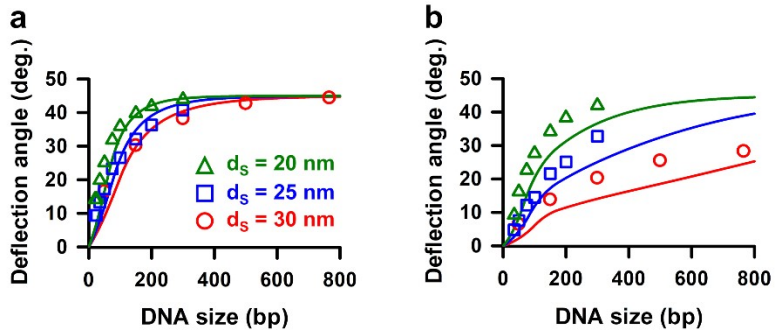

Supplementary Fig. S3. Analytical DNA stream deflection angle and comparison with experimental data depending on DNA size for varied nanochannel depths. (a-b) DNA deflection angle as a function of DNA size at d_D= 200 nm (a) and d_D= 50 nm (b). Symbols and solid lines are experimental data and analytical results, including electrostatic interaction between DNA and nanofilter. d_S= 30 nm (red circle), d_S= 25 nm (blue square) and d_S= 20 nm (green triangle).

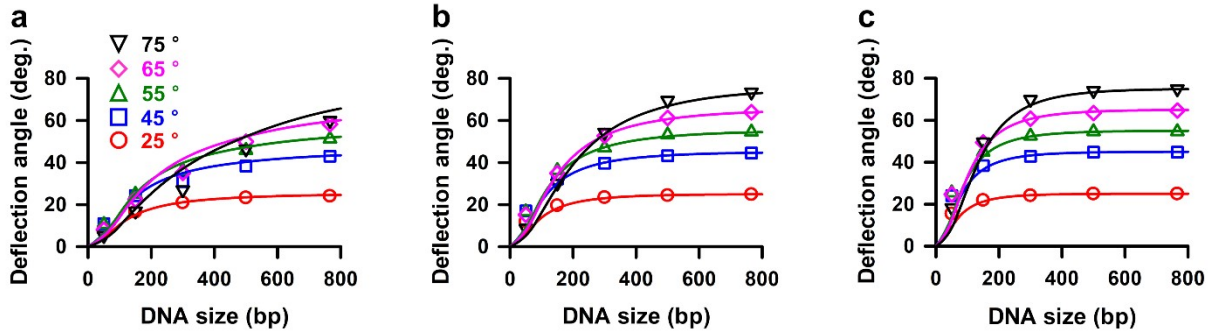

Supplementary Fig. S4. Analytical DNA stream deflection angle and comparison with experimental data depending on DNA size for varied nanofilter angles θ_N. (A-C) DNA deflection angle as a function of DNA size at d_S= 30 nm (a), d_S= 25 nm (b) and d_S= 20 nm (c). Symbols and solid lines are experimental data and analytical results, including electrostatic interaction between DNA and nanofilter. Nanofilter angle: 25° (open circle), 45° (open square), 55° (open triangle), 65° (open diamond) and 75° (open inverted triangle). Deep region depth and external field strength are 100 nm and 33.3 V/cm.

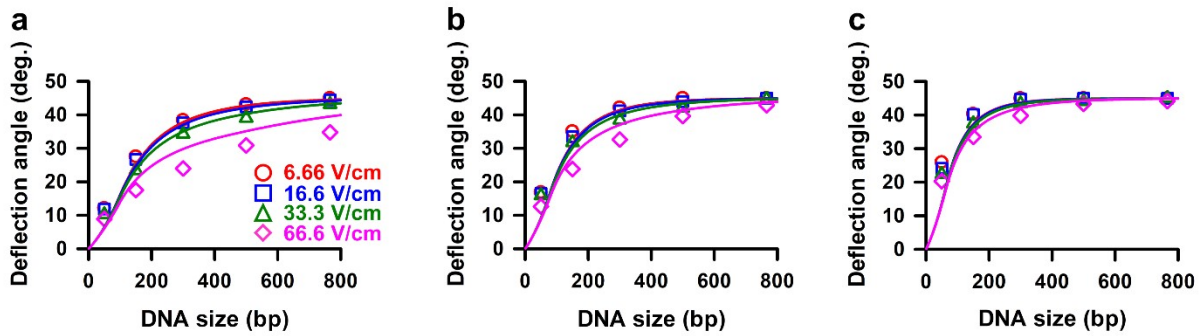

Supplementary Fig. S5. Analytical DNA stream deflection angle and comparison with experimental data depending on DNA size for varied external field strengths E_0. (a-c) DNA deflection angle as a function of DNA size at d_S= 30 nm (a), d_S= 25 nm (b) and d_S= 20 nm (c). Symbols and solid lines are experimental data and analytical results, including electrostatic interaction between DNA and nanofilter. External field strength: 6.66 V/cm (open circle), 16.6 V/cm (open square), 33.3 V/cm (open triangle) and 66.6 V/cm (open diamond). Deep region depth and nanofilter angle are 100 nm and 45°.

6. DNA stream deflection angles depending on nanofilter constriction size

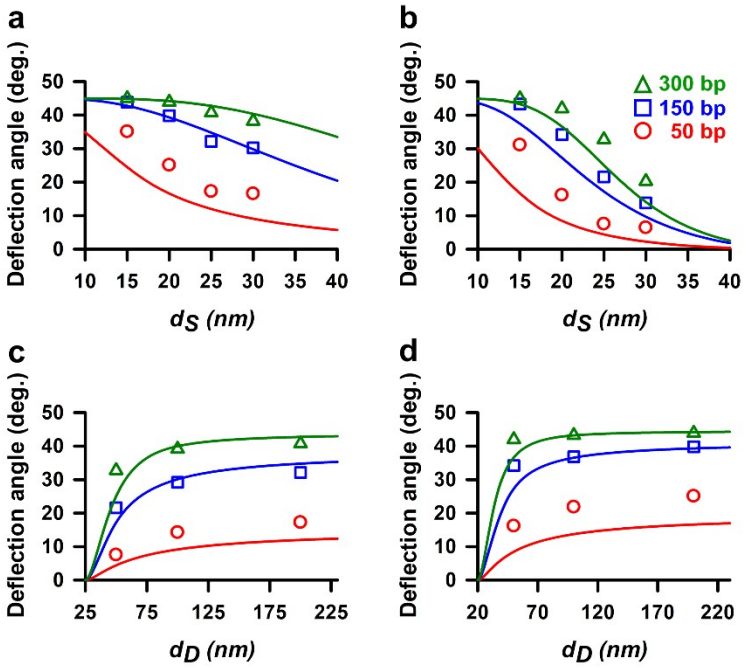

Supplementary Fig. S6. Analytical DNA stream deflection angle and comparison with experimental data for varied DNA sizes and nanochannel depths. (a-b) DNA deflection angle as a function of shallow region depth at d_D= 200 nm (a) and d_D= 50 nm (b). (c-d) DNA deflection angle as a function of deep region depth at d_S= 25 nm (c) and d_S= 20 nm (d). Nanofilter angle and external field strength are and 45° and 33.3 V/cm. Symbols and solid lines are experimental data and analytical results, including electrostatic interaction between DNA and nanofilter. DNA size: 50 bp (open circle), 150 bp (open square) and 300 bp (open triangle).

7. Theoretical DNA separation resolution in slanted nanofilter array

The separation resolution is defined by $R_{ij} = (x_j - x_i)/2\left(\Delta(L_{T\_i}) + \Delta(L_{T\_j})\right)$, where x_i and x_j are the peak distances and $\Delta(L_{T\_i})$ and $\Delta(L_{T\_j})$ are the standard deviations of the DNA dispersion in each DNA stream fitted with Gaussian curves. Theoretically, the peak distance is calculated using the travel distance L_T and deflection angle (Fig. 6a in main text), and the standard deviation $\Delta(L_T)$ is obtained from the asymptotic mean and variance of the molecule position. Suppose that a mixture of two DNAs of different lengths is subjected to a nanofilter. They have distinct deflection angles ($\theta_{M1} - \theta_E$ and $\theta_{M2} - \theta_E$) and dispersion ($\Delta_1(L_T)$, and $\Delta_2(L_T)$, which are defined by the standard deviation of DNA dispersion in each DNA stream at travel distance L_T from the same origin. We obtain the dispersion of DNA $\Delta(L_T)$ at travel distance L_T in the direction perpendicular to the DNA stream. The average speed of DNA along the stream is given by

$$v = \left\langle \frac{dx}{dt} \right\rangle \cos\theta_M + \left\langle \frac{dy}{dt} \right\rangle \sin\theta_M = \frac{w_S^+ w_D^+ (l_S + l_D)}{w_D^+ + w_S^+} \cos\theta_M + \frac{v_y^S w_D^+ + v_y^D w_S^+}{w_D^+ + w_S^+} \sin\theta_M \quad (31)$$

and the squared dispersion at time t is given by

$$\Delta^2(t) = \langle \Delta x^2 \rangle \sin^2\theta_M + \langle \Delta y^2 \rangle \cos^2\theta_M = \frac{w_S^+ w_D^+ \left(\left(w \right. \right.}{\left(\right.} \quad (32)$$

$$t\cos^2\theta_M$$

Using the relation $t = L_T/v$, we obtain $\Delta(L_T)$ as

$$\Delta^2(L_T) = \frac{w_S^+ w_D^+ \left(\left(w_D^+\right)^2 + \left(w_S^+\right)^2\right)(l_S + l_D)}{\left(w_D^+ + w_S^+\right)^2\left[w_S^+ w_D^+ (l_S + l_D)\cos\theta_M + \left(v_y^S\right.\right.} \quad (33)$$

where θ_M is given by Eq. (4) in main text.

8. Two limiting forms of the analytical solution

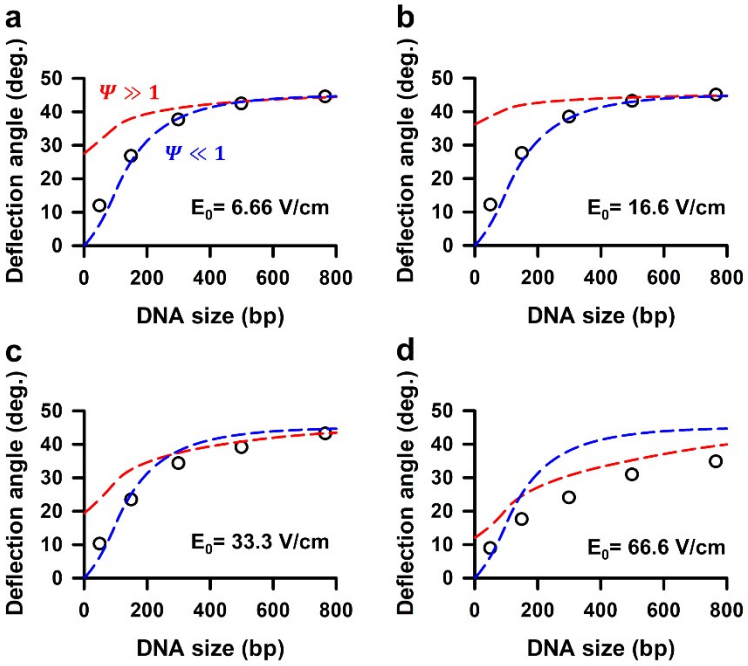

Supplementary Fig. S7. Analytical DNA stream deflection angle of two limiting forms ($\Psi \ll 1$ and $\Psi \gg 1$) and comparison with experimental data for varied external field strength at E_0= 6.66 V/cm (a), E_0= 16.6 V/cm (b), E_0= 33.3 V/cm (c) and E_0= 66.6 V/cm (d). Symbols and dotted lines are experimental data and analytical results of $\Psi \ll 1$ (blue color) and $\Psi \gg 1$ (red color). Nanofilter angle, shallow and deep region depths are θ_N= 45°, d_S= 30 nm and d_D= 100 nm.

References

1. Q. Pu, J. Yun, H. Temkin and S. Liu, *Nano Lett.*, 2004, **4**, 1099-1103.
2. S. H. Ko, D. Chandra, W. Ouyang, T. Kwon, P. Karande and J. Han, *Nat. Nanotechnol.*, 2017, **12**, 804-812.
3. H. Bow, J. Fu and J. Han, *Electrophoresis*, 2008, **29**, 4646-4651.
4. A. Brunet, C. Tardin, L. Salomé, P. Rousseau, N. Destainville and M. Manghi, *Macromolecules*, 2015, **48**, 3641-3652.
5. A. Savelyev, *Phys. Chem. Chem. Phys.*, 2012, **14**, 2250-2254.
6. W. Reisner, J. P. Beech, N. B. Larsen, H. Flyvbjerg, A. Kristensen and J. O. Tegenfeldt, *Phys. Rev. Lett.*, 2007, **99**, 058302.